Initial R-curves for Trans-laminar Fracture of Quasi-isotropic Carbon/Epoxy Laminates from Specimens with Increasing Size

Xiaodong Xu[1,2]*, Xiaoyang Sun[1], Michael R. Wisnom[1]

[1]Bristol Composites Institute, University of Bristol, University Walk, Bristol BS8 1TR, UK

[2] University of the West of England, Coldharbour Lane, Bristol BS16 1QY, UK

Abstract

In this paper, a set of initial R-curves were measured for three different in-plane sizes using scaled Over-height Compact Tension (OCT) specimens and two different stacking sequences. The data reduction scheme was based on a Virtual Crack Closure Technique which is informed by the measured failure load and effective crack length. The R-curve effects were studied by using X-ray Computed Tomography to measure the crack length throughout fracture propagation. It was found that the initial R-curves measured from all three specimen sizes follow the same linearly increasing trend, with similar results for both stacking sequences. However, no plateau was seen on any of the measured R-curves, implying that even the largest specimens are not large enough to generate a full R-curve.

Keywords: B. Fracture; B. Fracture toughness; D. X-ray computed tomography; R-curve

1. Introduction

Full-scale stiffened panels have been found to be tougher than expected on the basis of small coupon tests, and one key contributing factor is the existence of a fracture resistance curve, namely R-curve [1]. An R-curve describes the relationship between the fracture resistance, *R,* and the crack increment, Δ*a.* For composite materials, R-curves

*Corresponding author: xiaodong.xu@uwe.ac.uk (X. Xu)

have been reported for Mode I trans-laminar fracture [2-7] but different methods are used to determine values and the trends are not conclusive.

The definition and measurement of crack increments, Δa, is crucial for the determination of R-curves. However, there is not a single crack, but complex damage with multiple cracks in different plies. Some existing methods rely on optically measured crack length at the specimen surface [2] or the Digital Image Correlation (DIC) technique [4, 8]. Assumptions must be made to associate the surface measurements with the internal crack growth. Micron X-ray Computed Tomography (CT) has been adopted to better understand the internal damage states [9] and crack growth [10]. With CT images, damage and cracks in individual plies can be identified so the crack length can be defined and measured directly from experiments. Some indirect crack length determination methods have also been developed. For example, a Modified Compliance Calibration (MCC) method [3] used a linear elastic FE analysis to back-calculate the crack length at any measured compliance during fracture testing. A similar compliance based approach was also adopted by Ortega et al. [11]. However, these compliance-based methods ignore the Fracture Process Zone (FPZ) when determining the crack length. Bergan et al. [6] determined the crack increments indirectly using a cohesive law in an FE analysis, and the crack length also depends on the accuracy of the cohesive law which has its own assumptions.

The Over-height Compact Tension (OCT) test was developed by Kongshavn and Poursartip [12] to determine fracture properties of composite laminates. Damage development in OCT tests was investigated by Floyd [13], and Williams et al. [14]. Li et al. [15] carried out experimental investigations into OCT specimens including QI laminates with blocked central 0° ply. The damage progress was studied by using CT

2

scans and trans-laminar fracture toughness for fracture initiation was calculated using the ASTM E399 standard [16]. The initial machined notch length was used as the notch length, so no crack increments were considered. To apply DIC, Zobeiry [8] tested QI OCT specimens with surface 90° plies to minimize the surface damage, but the authors did not report an R-curve. Instead, the trans-laminar fracture toughness for failure propagation was taken as an average value by using an area method, and the crack increments were determined from the fracture process zone measurements from DIC [17]. So far, R-curves have not been experimentally measured using OCT specimens.

Effects of 0° ply thickness are important in determining the notched strength of composite laminates. Laffan et al. [18] investigated the ply thickness effect on trans-laminar fracture toughness, and attributed the differences to the pull-out of the fibres in the 0° ply blocks of different thicknesses. Ortega et al. [19] studied the ply thickness effect on cohesive laws of different hybrid laminates using compact tension tests. They found that blocked 0° plies resulted in a tougher response. These stacking sequence effects on notched tensile strength and trans-laminar fracture toughness related to the thickness of the 0° plies are caused by splitting and its resulting stress blunting effect. Among the notched configurations, Quasi-isotropic (QI) stacking sequences are widely used in real-world applications, owing to their balanced performance in all directions. Li et al. [15] reported different trans-laminar fracture toughness values for IM7/8552 QI layups with different ply block thicknesses ($[45/90/-45/0]_{4s}$, $[45_2/90_2/-45_2/0_2]_{2s}$ and $[45_4/90_4/-45_4/0_4]_s$) with the blocked-ply laminates being tougher. Xu et al. [20] reported that the blocked-ply IM7/8552 QI laminates with a thicker central 0° ply ($[45_2/90_2/-45_2/0_2]_{2s}$) are tougher than those without ($[90_2/45_2/0_2/-45_2]_{2s}$), yet the dispersed plies ($[45/90/-45/0]_{4s}$ and $[90/45/0/-45]_{4s}$) exhibited a similar trans-laminar fracture toughness

3

during initial fracture propagation in the OCT tests. This is because the $[45_2/90_2/-45_2/0_2]_{2s}$ laminate has half the 0° plies blocked at the centre, which generates a much tougher response than the $[90_2/45_2/0_2/-45_2]_{2s}$ laminate. However, the $[45/90/-45/0]_{4s}$ laminate only has a quarter of the 0° plies blocked at the centre, so the initial fracture response is similar to the $[90/45/0/-45]_{4s}$ laminate, which is mainly controlled by the single 0° plies. Since only the trans-laminar fracture toughness values for initial fracture propagation were compared between $[45/90/-45/0]_{4s}$ and $[90/45/0/-45]_{4s}$ laminates in [20], it is not clear if the 0° ply thickness affects the results as the crack propagates further into the tests and more damage is present.

In this work, initial R-curves were measured carefully using a complete set of scaled OCT specimens. Three in-plane sizes, i.e., scaled-down (53 mm by 104 mm), baseline (106 mm by 208 mm) and scaled-up (212 mm by 416 mm), were used to check if the measured initial R-curves are size-dependent and whether the specimens are large enough. The extensive test programme also included two different QI stacking sequences, i.e., $[90/-45/0/-45]_{4s}$ and $[45/90/-45/0]_{4s}$ which were used to study the effect of the central double 0° ply. Fracture propagation was examined throughout the OCT tests, and the crucial crack increments were measured using CT scans of multiple specimens from interrupted tests. As a result, the current crack measurement method is objective and is based on internal damage from CT scans rather than surface measurements or compliance.

The objective of this study is to gain a fundamental understanding of trans-laminar fracture toughness which can be used to develop and validate methods for numerical modelling based on a sound foundation. It was found that the initial R-curves show the same linearly increasing trend for all sizes and are not significantly influenced by the

4

central double 0° ply considering experimental scatter. No plateau is seen on the measured initial R-curves even with the scaled-up OCT tests.

2. Experimental Studies

2.1 Test Setup

The OCT specimens with three in-plane dimensions are shown in Fig. 1a. Three specimens were tested until failure for each case. All in-plane dimensions of the scaled-down OCT specimen are half of those in the baseline OCT specimen as shown in Fig. 1b. All in-plane dimensions of the scaled-up OCT specimen are doubled from those in the baseline OCT specimen. The in-plane scaled OCT specimens were tested in a hydraulic-driven Instron 100 kN test machine under displacement control at a rate of 0.5 mm/min for the scaled-down, 1 mm/min for the baseline and 2 mm/min for the scaled-up case, respectively. No anti-buckling rods were attached to the rear end of scaled-down OCT specimen as no buckling failure was observed, but anti-buckling rods and upgraded anti-buckling guides were used for the larger OCT specimens. Interrupted tests in which each specimen was unloaded after certain load drops (2 to 3 load levels) on the respective load-POD curves were carried out to study the failure mechanisms via CT scanning. The specimens from the interrupted tests were soaked in a bath of zinc iodide penetrant for at least 3 days. A Nikon XTH 225ST CT scanner was used for damage evaluation. It has a 225kV, 225W microfocus X-ray source and a 3-micron focal spot size.

The material used was Hexcel's HexPly® IM7/8552 carbon/epoxy pre-preg with a 0.125 mm nominal cured ply thickness. To form a complete set, new OCT tests are conducted in addition to the previous OCT tests. For the [45/90/-45/0]4s stacking sequence, all test results of the baseline, scaled-down and scaled-up OCT specimens

were reported previously in [9]. For the [90/45/0/-45]4s stacking sequence, only results

of the scaled-down OCT specimens were conducted in [21], while those of the baseline

and scaled-up OCT specimens are new.

2.2 Experimental Results

In all OCT tests, the loads increased linearly at the beginning. Then fracture in front

of the notch occurred when significant load drops appear on the load-POD curves. All

specimens suffered compressive failure at their rear ends at the final stage of the tests.

The experimental load-POD curves from the scaled-down, baseline and scaled-up OCT

tests are shown in Fig. 2.

The load-POD curves for different layups are similar for each size as shown in Fig.

2. The difference between layups is not significant considering the experimental scatter.

This will be explained in the following section through CT scan analyses. The initial

slopes vary slightly in Fig. 2c. This is partially because one specimen was initially

loaded up to a high load before buckling occurred, and then it was reloaded after

improvements were done to the test set-up to avoid buckling as shown in Fig. 3.

Damage was therefore expected to exist in that specimen after the initial loading, so the

slope in the second attempted test shown in Fig. 2c is less steep than the other tests. In

Fig. 3, two thick steel plates were directly fixed to the test machine and then gently

clamped the specimen rear end to stop torsional buckling in the scaled-up OCT tests, as

compared to the previous anti-bucking rods attached to the specimen itself as shown in

Fig. 1a. The improvement was successful, as the buckling was prevented in the scaled-

up [90/45/0/-45]$_{4s}$ OCT tests and the loads were reduced to almost zero at the end of the

tests. However, in the previous scaled-up [45/90/-45/0]$_{4s}$ OCT tests, buckling occurred

6

at the specimen rear end in all three tests, so the tests were stopped shortly after the peak loads were achieved.

3. Results Analysis

3.1 CT Analyses

By checking the CT images from interrupted tests in Figures 4 to 9, the damage states in the laminates with different layups and dimensions after similar load drops were compared. The crack increments in the 0° plies at the interrupted load levels were measured at the machined notch tip.

Comparing Fig. 4a and b against Fig. 4c and d at the first large load drop (marked in Fig. 2 with the interrupted loads reported in caption of Fig. 4), the initial fracture propagation in the scaled-down OCT tests is studied through CT scan images. The 0° splitting was found to be longer in the central double 0° ply with 45° surface plies in Fig. 4a than in the single 0° plies for both stacking sequences in Fig. 4b and 4d, which have been reported to blunt stress concentrations [22, 23], leading to a tougher response. However, for the current 4 mm thick specimen, the double central 0° ply only counts for ¼ of the total 0° plies, so it does not to lead to a significantly tougher laminate according to [24]. The fibre breakage in all single 0° plies is similar as shown in Fig. 4b and 5d. The scaled-down OCT specimen with surface 90° plies does not have a double central 0° ply, but it has a double central -45° ply instead. There is no fibre fracture in this ply, due to delamination present as seen in Fig. 4c. The same applies to the baseline OCT specimens with both stacking sequences interrupted after the first large load drop as shown in Fig. 5, and the scaled-up OCT specimens with both stacking sequences as shown in Fig. 6.

7

In Fig. 7, the damage ahead of the machined notch tip was examined after the tests were stopped at the major load drops around the peak loads (marked in Fig. 2 with the interrupted loads reported in the caption of Fig. 7) to study further fracture propagation in the scaled-down OCT tests. While the fibre breakage grows ahead of the notch tip perpendicular to the loading direction, the damage height grows significantly in the loading direction. The growth of damage height contributes to an increase of trans-laminar fracture energy. With surface 45° plies, the splitting and delamination in the central double 0° ply in Fig. 7a grow much longer than those in the outboard single 0° plies in Fig. 7b. Such long 0° splitting contributes to a large damage height that can significantly blunt the stress concentration. This will lead to a tougher response at the specimen central double 0° ply. However, only accounting for ¼ of the total 0° plies, it does not to lead to a significantly tougher laminate according to [24]. By comparison, in the laminates with surface 90° plies, the fibre fracture in the single 0° plies in Fig. 7d is similar to that in the outboard single 0° ply with surface 45° plies in Fig.7b. The delamination in the central -45° ply also grows significantly along the -45° splits as seen in Fig. 7c and has such a significant stress blunting effect that no fibre failure was observed in that ply. The same also applies to the baseline OCT specimens with both stacking sequences interrupted at the major load drops around the peak loads as shown in Fig. 8, and the scaled-up OCT specimens with both stacking sequences as shown in Fig. 9. Because the sample sizes are larger, and the failure loads are higher than those in the scaled-down OCT tests, the damage grows even further.

The damage state was observed at a further load drop later in the scaled-up OCT tests (marked in Fig. 2 with the interrupted loads reported in caption of Fig. 10). The damage height is as high as 50 mm (Fig. 10a) while the crack increment in the single 0° plies is

over 30 mm (Fig. 10b). However, these results should be discarded as the crack length is too large for the specimen size according to ASTM D5045 standard [25].

The crack increments in the 0° plies are measured from the CT images. This was based on the definition of effective crack increments [21] and is simply referred to as crack increments in this paper. The average crack increments of the 0° plies at the different interrupted load levels for the three sizes and two layups are listed in Table 1.

3.2 Data Reduction Method

The load-displacement response is not smooth, but involves many load drops making it difficult to use a purely experimental approach to determine the fracture energy from the compliance of the OCT specimens. A Virtual Crack Closure Technique (VCCT) analysis in a Linear Elastic Finite Element (LEFE) model in Abaqus Standard was therefore used for characterising the fracture energy. An FE model of the OCT specimen geometry was built as shown in Fig. 11. The OCT specimen as shown in Fig. 1b has a doubled height compared to the compact tension specimen from the ASTM E399 [16] and ASTM D5045 [25] standards. The VCCT determined fracture energy values based on the experimentally measured failure load and crack increments were used to generate R-curves. The measured crack increments are based on the fibre breakage length in the 0° plies which effectively includes a damage process zone, which will be discussed further in the next section. As a result, the nonlinearity due to this damage has been accounted for in the current VCCT analysis.

The material properties used in the model are homogeneous elastic isotropic, with E = 61.6 GPa and Poisson's ratio, v = 0.3. 8-noded continuum elements (C3D8) were used with one element through the thickness. A sensitivity study was carried out to study the effect of the mesh size (2 mm, 1 mm, 0.5 mm and 0.2 mm). The results suggested that a

0.5 mm uniform mesh is sufficient for the VCCT analysis, which yielded almost the same predicted load at a given strain energy release rate as the 0.2 mm uniform mesh. For boundary constraints, displacements were applied at the pairs of nodes representing the centre of the upper loading pin and all translational degree of freedoms were fixed at the nodes representing the centre of the lower loading pin. The pins themselves were not modelled.

In Abaqus VCCT analysis, a path was defined through a bonded node set in the Abaqus VCCT analysis which corresponds to the crack. The predictive Abaqus VCCT analysis is done inversely compared to the conventional VCCT analysis. A strain energy release rate, G, is needed as an input rather than an output. Therefore, an estimated G at the experimentally measured load and crack increment are needed, and the predicted crack propagation load needs to be compared with the experimental failure load to see if the estimation is reasonable. If there is a discrepancy, the estimated G needs to be revised iteratively until an agreement is reached, and the input G can be regarded as G_C at the measured crack increment. Here, the initial G estimation is done by introducing an adjustment factor to the ASTM D5045 standard data reduction method which is intended for the different compact tension specimen. It was found that for a given G value the FE predicted load is about 8% higher than the calculated load as per the ASTM D5045 standard. By conducting the above iterative VCCT analysis in Abaqus, the R-curve for the OCT configuration was derived.

3.3 R-curves

The definition of crack length is very important for the construction of R-curves but is difficult to determine due to the complex nature of the damage compared to a sharp crack. Here, the effective crack length defined by Xu et al. [21] is used which is based

on the crack increments in the 0° plies, and is called crack length in this paper for simplicity. This includes the process zone where there are still intact ±45° plies, and is longer than the through-thickness crack where all plies are broken. The R-curve derived based on the effective crack length was referred to as an effective R-curve [21], and in this paper is simply called the R-curve.

When deriving the R-curve, it is impossible to interrupt the tests just before the load drop and measure the crack increments. Therefore, the crack increments were measured right after the load drops while the loads were taken at the load drops. The assumption is that the fibre fracture in the 0° plies does not change after the load drop, but it is the ±45° plies that are broken, which turns a damage process zone (0° plies broken but ±45° plies intact) into a through-thickness crack (all plies broken). The crack length based on the 0° plies therefore does not change just before or after the load drop. This is supported by a comparison of the CT scan images from previous notched tests. In OCT tests of the same IM7/8552 [45/90/-45/0]$_{4s}$ laminates in [9], the tests were interrupted after the first large load drop in which all plies were broken. In earlier centre-notched tests of the same material and stacking sequence in [23], failure occurred suddenly, with a single load drop. The tests were interrupted just before the ultimate load drop and only 0° plies were observed to be broken, but not ±45° plies. The fibre breakage length in the 0° plies was similar to that in [9], suggesting that only ±45° plies are broken during the load drop.

The data that can be used to construct an R-curve are two data points for each specimen size and layup due to the available number of valid interrupted test results. A third data point can be interpreted at zero crack increment under the assumption that crack initiation does not take place up to the first visible load drop on the load-

11

displacement curves. Hence the load value at the first visible load drop was extracted from Fig. 2, which occurs before the labelled first large load drop. The average from the three samples was taken and is labelled with open symbols in Fig. 12. In contrast, the load values for the other data points on the R-curve were from the individual interrupted tests used for CT scanning and crack increment measurements.

For the determination of R-curves, the crack length, a, should not exceed a certain value determined by Eq. 1 according the ASTM D5045 standard [25].

$$W - a > 2.5 (\frac{K_{IC}}{\sigma_u})^2 \tag{1}$$

where σ_u is the unnotched strength of 990 MPa for the same material and QI laminate [26]. Fracture energy (G_{IC}) can be calculated from fracture toughness, K_{IC}, via the following equation assuming plane stress.

$$G_{Ic} = \frac{K_{IC}^2}{E} \tag{2}$$

where G_{IC} is the fracture energy, K_{IC} is the fracture toughness and E is the Young's modulus.

Substituting K_{IC} with G_{IC} according to Eq. 2 and re-arranging Eq. 1, we have Eq. 3 for the maximum permissible crack length.

$$a < W - 2.5 \frac{G_{IC}E}{\sigma_u^2} \tag{3}$$

Fig. 12 shows the R-curves with three data points as per the VCCT based data reduction method for each specimen size and layup. The invalid points according to Eq. 3 are excluded because the crack increment, is too large for the specimen size, i.e. after the major load drop for the scaled-down OCT specimens (5.4 mm crack increment), and for the further load drop for the scaled-up OCT specimens (34.5 mm crack increment).

Then all R-curves approximately fall on the same line. The measured R-curves were found to be similar for the two QI layups.

The scaled-down OCT specimens were already found to be too small to generate a fully-developed damage zone [9]. The baseline and the scaled-up specimens are more suitable to measure the R-curve, with the scaled-up specimen being able to generate more crack growth before the crack length is too large even for the largest specimen geometry. None of the measured R-curves have shown a plateau yet.

4. Discussion

It needs to be noted that multiple samples of the same configuration from different interrupted tests were used to construct the R-curve, rather than a single sample. Such a limitation of the current method is due to the necessity of using dye penetrant for CT scanning of the large OCT specimens to enhance the contrast in the images. Once dye penetrant is applied, the same sample cannot be re-used because of the potential interference with the fracture properties. The current method can be improved by using *in situ* CT scanning. This has been successfully applied to small specimens and showed a similar trend of linearly increasing fracture energy with initial crack length for a different material [10], but needs further development for large specimens and to capture the internal damage right at the load drop.

None of the measured R-curves in this paper have yet shown a plateau. This however contradicts other papers based on $[90/0]_{ns}$ cross-ply laminates which record a plateau value for the R-curves [2, 4, 5] under tension. This is not surprising because multi-directional laminates have larger and more complex damage patterns compared to cross-ply laminates. Among limited published data, some methods have predicted a plateau for R-curves of multi-directional laminates [5, 6, 27]. For example, centre-notched

IM7/8552 specimens [5] or scaled edge notched QI-T700/AR-2527 NCF QI specimens [27] were used to derive R-curves for multidirectional laminates. The failure of these specimens was unstable, so the results were indirectly used to estimate the R-curves via the contribution of their 0° plies [5] or a size effect law [27]. Test data for large crack increments in these multidirectional laminates were missing. In [6] for a AS4/VRM-34 $[\pm45/90_2/0/90_2/\pm45]_s$ laminate, a plateau of the R-curve was simulated in an FE analysis, but no experimentally derived R-curves were reported. It is unclear when a plateau value might be measured for the R-curve of the current IM7/8552 QI laminates, which needs to be investigated using even larger specimens such as the large-scale panel tests in [1, 28]. In addition to the two QI layups tested, more tests on a wider range of QI stacking sequences would be valuable.

5. Conclusions

The R-curves of in-plane scaled Over-height Compact Tension (OCT) carbon/epoxy laminates were characterized by using a combination of experiments, VCCT analysis, and X-ray Computed Tomography (CT). The initial R-curves from all sizes and two layups follow the same linearly increasing trend without reaching a plateau. The implication is that the initial R-curve is size independent and not very sensitive to stacking sequence.

The scaled-down OCT specimen is less suitable for the determination of R-curves than the baseline and the scaled-up OCT specimens. This is because the scaled-down OCT specimen can only generate limited crack growth before it exceeds the acceptable range relevant to the specimen size. However, even in the largest OCT tests, the damage height grows extensively at the end of the test. Since the measured initial R-curves have

not shown a plateau owing to extensive damage, none of the specimens are large enough to generate a full R-curve.

Both QI layups have similar initial R-curves within the limits of experimental accuracy, despite one having a double central 0° ply which sees greater stress blunting from the longer central double 0° splits. This is because the tougher central double 0° ply only counts for a quarter of the 0° plies, so its contribution is not that significant. The majority of the 0° plies are the single 0° plies which behave similarly in both QI layups.

References

[1] X. Xu, S. Takeda, Y. Aoki, S.R. Hallett, M.R. Wisnom, Predicting notched tensile strength of full-scale composite structures from small coupons using fracture mechanics, Composite Structures 180 (2017) 386-394.

[2] S.T. Pinho, P. Robinson, L. Iannucci, Fracture toughness of the tensile and compressive fibre failure modes in laminated composites, Composites Science and Technology 66(13) (2006) 2069-2079.

[3] M.J. Laffan, S.T. Pinho, P. Robinson, L. Iannucci, Measurement of the in situ ply fracture toughness associated with mode I fibre tensile failure in FRP. Part I: Data reduction, Composites Science and Technology 70(4) (2010) 606-613.

[4] G. Catalanotti, P.P. Camanho, J. Xavier, C.G. Dávila, A.T. Marques, Measurement of resistance curves in the longitudinal failure of composites using digital image correlation, Composites Science and Technology 70(13) (2010) 1986-1993.

[5] P.P. Camanho, G. Catalanotti, On the relation between the mode I fracture toughness of a composite laminate and that of a 0° ply: Analytical model and experimental validation, Engineering Fracture Mechanics 78(13) (2011) 2535-2546.

[6] A. Bergan, C. Dávila, F. Leone, J. Awerbuch, T.-M. Tan, A Mode I cohesive law characterization procedure for through-the-thickness crack propagation in composite laminates, Composites Part B: Engineering 94 (2016) 338-349.

[7] R.F. Teixeira, S.T. Pinho, P. Robinson, Thickness-dependence of the translaminar fracture toughness: Experimental study using thin-ply composites, Composites Part A: Applied Science and Manufacturing 90 (2016) 33-44.

[8] N. Zobeiry, R. Vaziri, A. Poursartip, Characterization of strain-softening behavior and failure mechanisms of composites under tension and compression, Composites Part A: Applied Science and Manufacturing 68(0) (2015) 29-41.

[9] X. Xu, M.R. Wisnom, Y. Mahadik, S.R. Hallett, Scaling of fracture response in over-height compact tension tests, Composites Part A: Applied Science and Manufacturing 69(0) (2015) 40-48.

[10] X. Sun, S. Takeda, M.R. Wisnom, X. Xu, In situ characterization of trans-laminar fracture toughness using X-ray Computed Tomography, Composites Communications 21 (2020) 100408.

[11] A. Ortega, P. Maimí, E.V. González, D. Trias, Characterization of the translaminar fracture Cohesive Law, Composites Part A: Applied Science and Manufacturing 91 (2016) 501-509.

[12] I. Kongshavn, A. Poursartip, Experimental investigation of a strain-softening approach to predicting failure in notched fibre-reinforced composite laminates, Composites Science and Technology 59(1) (1999) 29-40.

[13] A.M. Floyd, An engineering approach to the simulation of gross damage development in composites laminates, Department of Civil Engineering, PhD Thesis, The University of British Columbia, Vancouver, Canada, 2004.

[14] K.V. Williams, R. Vaziri, A. Poursartip, A physically based continuum damage mechanics model for thin laminated composite structures, International Journal of Solids and Structures 40(9) (2003) 2267-2300.

[15] X. Li, S.R. Hallett, M.R. Wisnom, N. Zobeiry, R. Vaziri, A. Poursartip, Experimental study of damage propagation in Over-height Compact Tension tests, Composites Part A: Applied Science and Manufacturing 40(12) (2009) 1891-1899.

[16] ASTM, Standard, E399-90, Standard test method for plane-strain fracture toughness of metallic materials, ASTM International, West Conshohocken, PA, USA, 1990 (1997).

[17] N. Zobeiry, Extracting the strain-softening response of composites using full-field displacement measurement, Department of Civil Engineering, PhD Thesis, The University of British Columbia, Vancouver, 2010, p. 198.

[18] M.J. Laffan, S.T. Pinho, P. Robinson, L. Iannucci, Measurement of the in situ ply fracture toughness associated with mode I fibre tensile failure in FRP. Part II: Size and lay-up effects, Composites Science and Technology 70(4) (2010) 614-621.

[19] A. Ortega, P. Maimí, E.V. González, J.R. Sainz de Aja, F.M. de la Escalera, P. Cruz, Translaminar fracture toughness of interply hybrid laminates under tensile and compressive loads, Composites Science and Technology 143 (2017) 1-12.

[20] X. Xu, M.R. Wisnom, S.R. Hallett, N. Zobeiry, S. Leslie, A. Poursartip, R. Vaziri, Stacking sequence effects in over-height compact tension tests of quasi-isotropic laminates, 19th International Conference on Composite Materials, Montreal, Canada, 2013.

[21] X. Xu, M.R. Wisnom, S.R. Hallett, Deducing the R-curve for trans-laminar fracture from a virtual Over-height Compact Tension (OCT) test, Composites Part A: Applied Science and Manufacturing 118 (2019) 162-170.

[22] S.R. Hallett, B.G. Green, W.G. Jiang, M.R. Wisnom, An experimental and numerical investigation into the damage mechanisms in notched composites, Composites Part A: Applied Science and Manufacturing 40(5) (2009) 613-624.

[23] X. Xu, M.R. Wisnom, Y. Mahadik, S.R. Hallett, An experimental investigation into size effects in quasi-isotropic carbon/epoxy laminates with sharp and blunt notches, Composites Science and Technology 100(0) (2014) 220-227.

[24] X. Xu, A. Paul, M.R. Wisnom, Thickness effect on Mode I trans-laminar fracture toughness of quasi-isotropic carbon/epoxy laminates, Composite Structures 210 (2019) 145-151.

[25] ASTM, Standard, D5045-14, Standard Test Methods for Plane-Strain Fracture Toughness and Strain Energy Release Rate of Plastic Materials, ASTM International, West Conshohocken, PA, USA, 2014.

[26] X. Xu, M.R. Wisnom, K. Chang, S.R. Hallett, Unification of strength scaling between unidirectional, quasi-isotropic, and notched carbon/epoxy laminates, Composites Part A: Applied Science and Manufacturing 90 (2016) 296-305.

[27] G. Catalanotti, A. Arteiro, M. Hayati, P.P. Camanho, Determination of the mode I crack resistance curve of polymer composites using the size-effect law, Engineering Fracture Mechanics 118 (2013) 49-65.

[28] A. Bergan, J. Bakuckas Jr, J. Awerbuch, T.-M. Tan, Assessment of damage containment features of a full-scale PRSEUS fuselage panel, Composite Structures 113 (2014) 174-185.

(a) Scaled OCT test set-up   (b) Baseline geometry
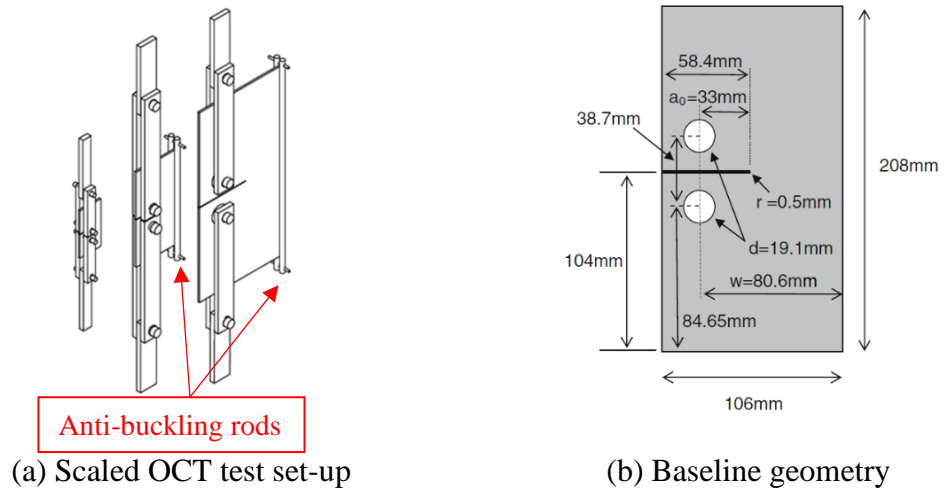
Fig. 1. OCT test set-up and specimen dimensions.
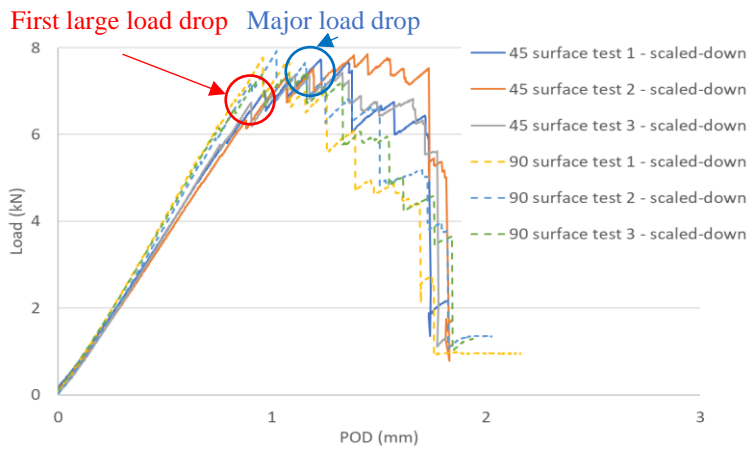
(a) Load-POD curves from the scaled-down OCT tests.
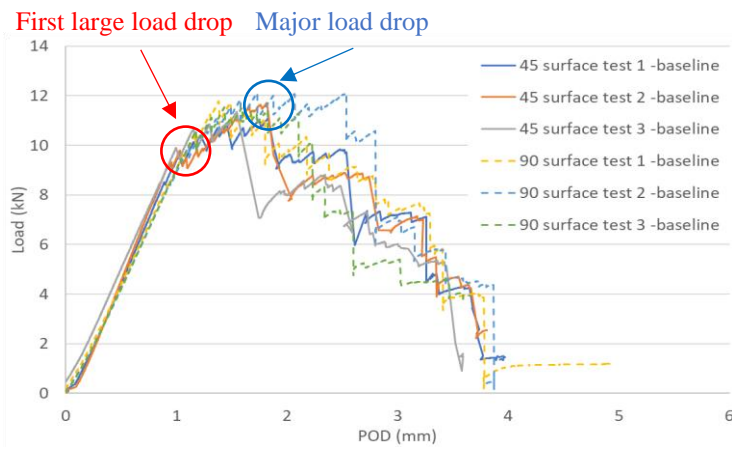
(b) Load-POD curves from the baseline OCT tests.
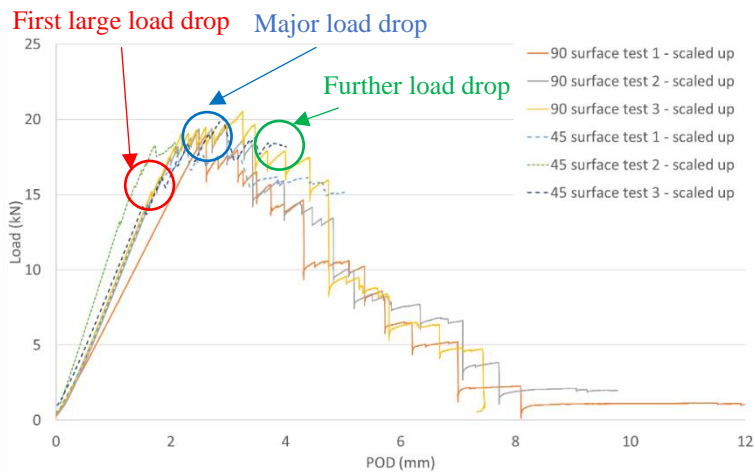
(c) Load-POD curves from the scaled-up OCT tests.

Fig. 2. OCT test results.
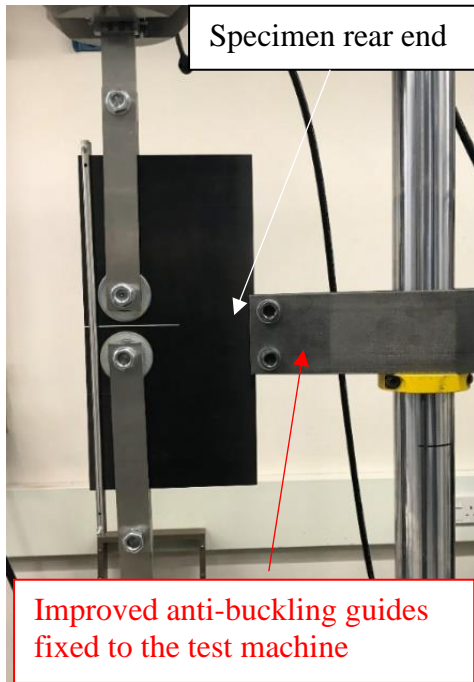
Fig. 3. Improved anti-buckling measures in the scaled-up OCT tests.
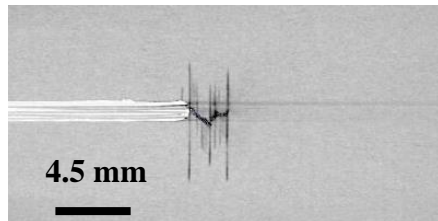
(a) [45/90/-45/0]$_{4s}$, Central double 0° ply, 6.9 kN
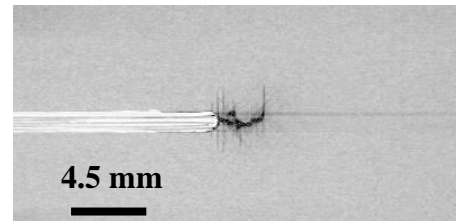
(b) [45/90/-45/0]$_{4s}$, Single 0° ply, 6.9kN
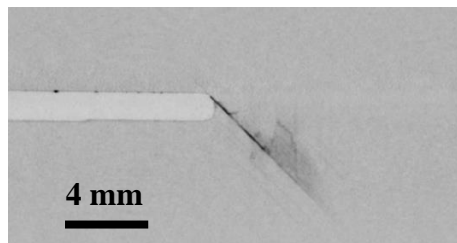
(c) [90/45/0/-45]$_{4s}$, Central double -45° ply, 6.8 kN
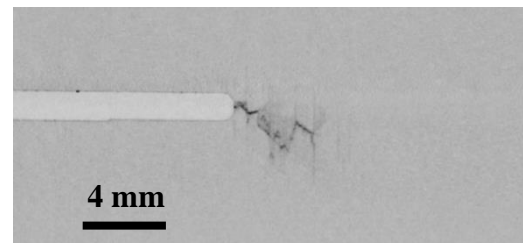
(d) [90/45/0/-45]$_{4s}$, Single 0° ply, 6.8 kN

Fig. 4. CT images of the scaled-down OCT specimens after the first large load drop.
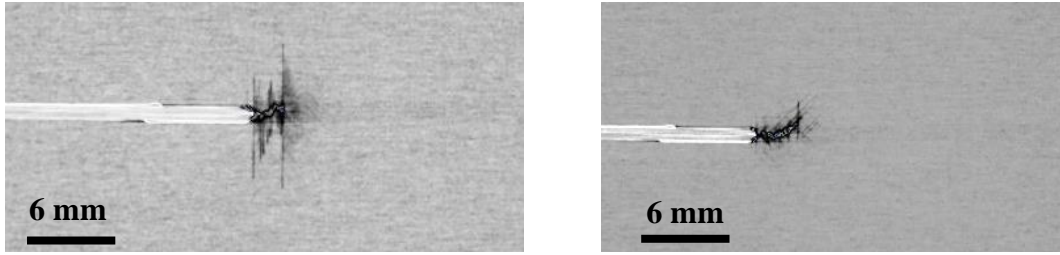
(a) [45/90/-45/0]$_{4s}$, Central double 0° ply, 9.9 kN   (b) [45/90/-45/0]$_{4s}$, Single 0° ply, 9.9 kN
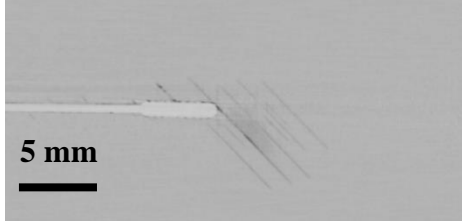
(c) [90/45/0/-45]$_{4s}$, Central double -45° ply, 10.1 kN (d) [90/45/0/-45]$_{4s}$, Single 0° ply, 10.1 kN

Fig. 5. CT images of the baseline OCT specimens after the first large load drop.

(a) [45/90/-45/0]$_{4s}$, Central double 0° ply, 14.2 kN   (b) [45/90/-45/0]$_{4s}$, Single 0° ply, 14.2 kN
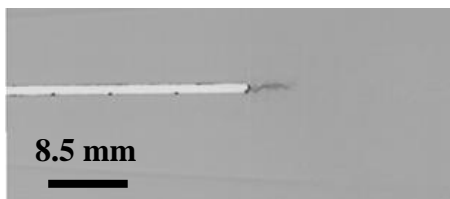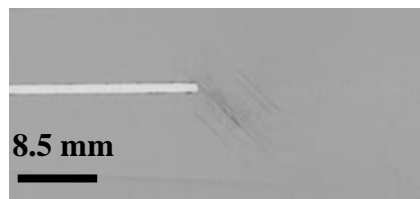
(c) [90/45/0/-45]$_{4s}$, Central double -45° ply, 16.5 kN (d) [90/45/0/-45]$_{4s}$, Single 0° ply, 16.5 kN

Fig. 6. CT images of the scale-up OCT specimens after the first large load drop.
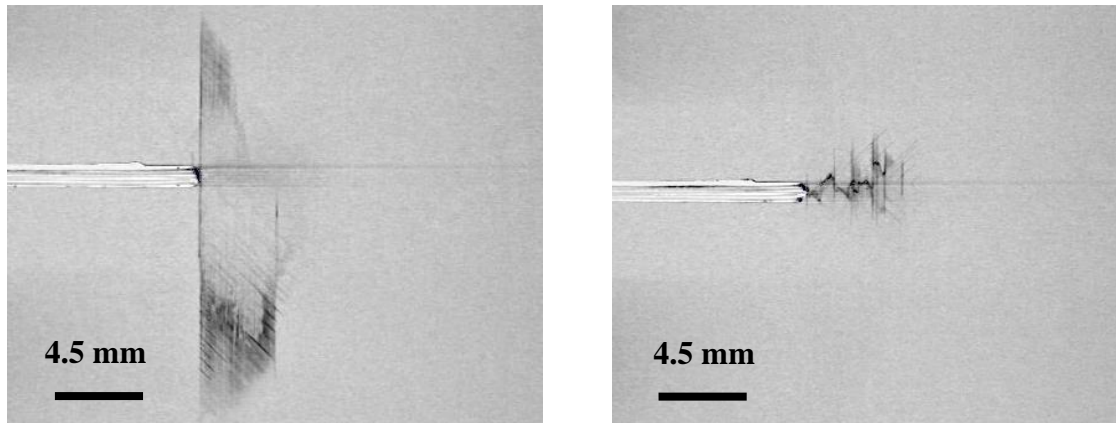
(a) [45/90/-45/0]$_{4s}$, Central double 0° ply, 7.4 kN   (b) [45/90/-45/0]$_{4s}$, Single 0° ply, 7.4 kN

Dye penetrant residue
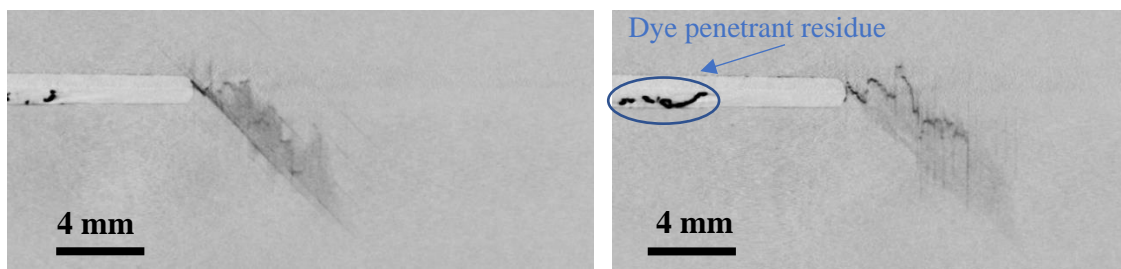
(c) [90/45/0/-45]$_{4s}$, Central double -45° ply, 7.6 kN (d) [90/45/0/-45]$_{4s}$, Single 0° ply, 7.6 kN

Fig. 7. CT images of the scaled-down OCT specimens after the major load drop.
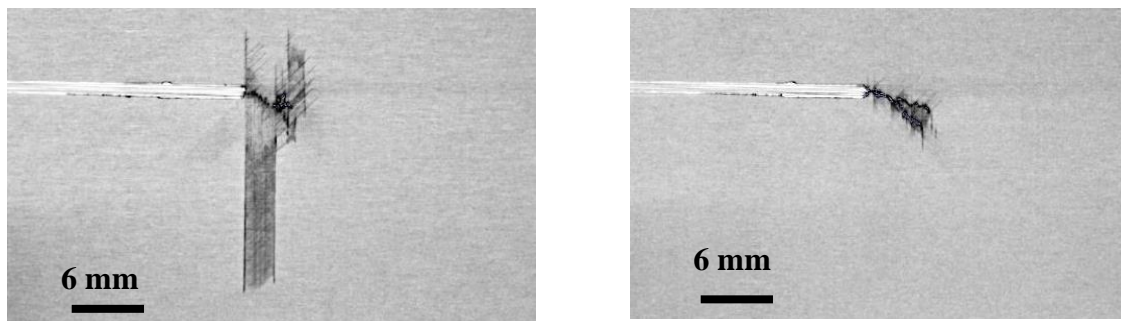
(a) [45/90/-45/0]$_{4s}$, Central double 0° ply, 11.2 kN   (b) [45/90/-45/0]$_{4s}$, Single 0° ply, 11.2 kN
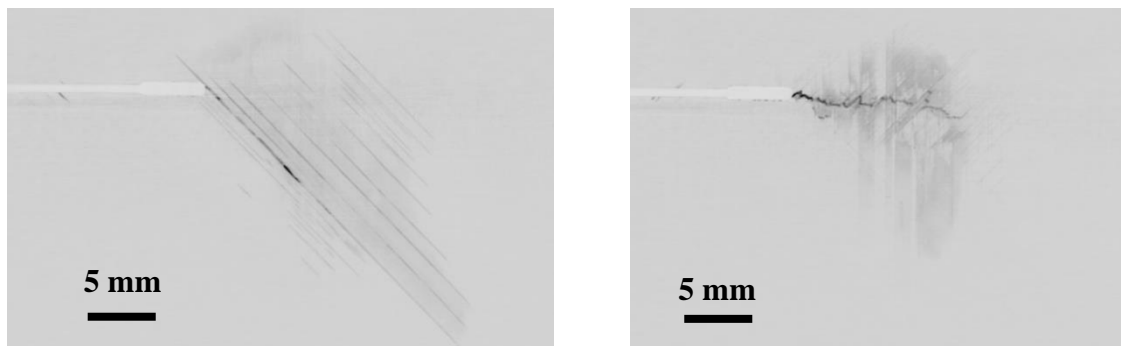
(c) [90/45/0/-45]$_{4s}$, Central double -45° ply, 10.8 kN (d) [90/45/0/-45]$_{4s}$, Single 0° ply, 10.8 kN

Fig. 8. CT images of the baseline OCT specimens after the major load drop.
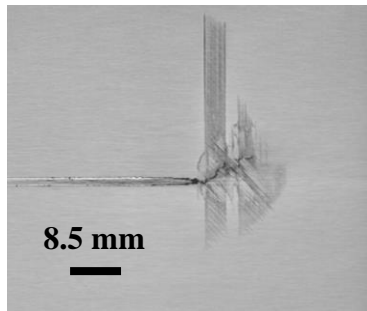
(a) [45/90/-45/0]$_{4s}$, Central double 0° ply, 18.5 kN
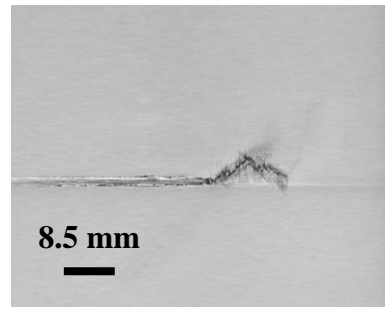
(b) [45/90/-45/0]$_{4s}$, Single 0° ply, 18.5 kN
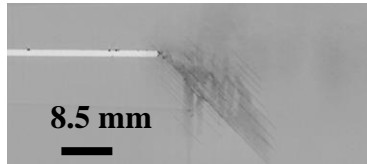
(c) [90/45/0/-45]$_{4s}$, Central double -45° ply, 18.9 kN
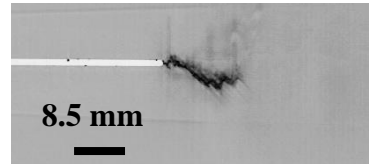
(d) [90/45/0/-45]$_{4s}$, Single 0° ply, 18.9 kN

Fig. 9. CT images of the scaled-up OCT specimens after the major load drop.
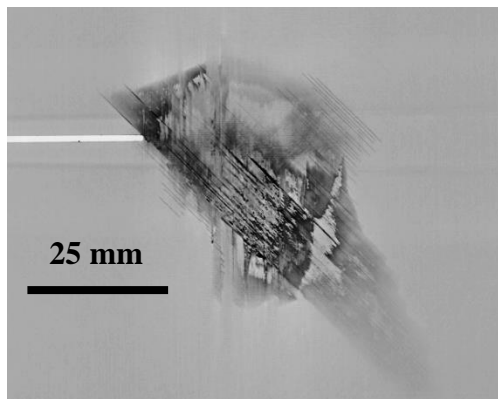
(a) Central double -45° ply
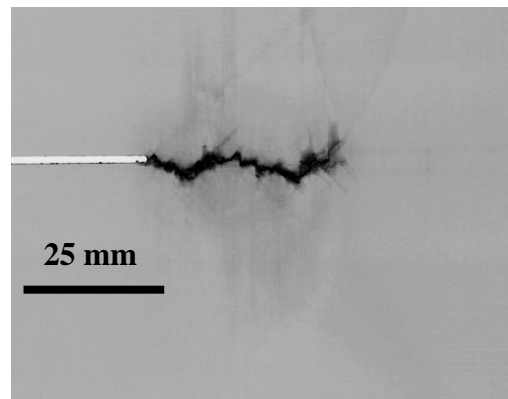
(b) Single 0° ply

Fig. 10. CT images of the [90/45/0/-45]$_{4s}$ scaled-up OCT specimen further into the test at 19.6 kN.
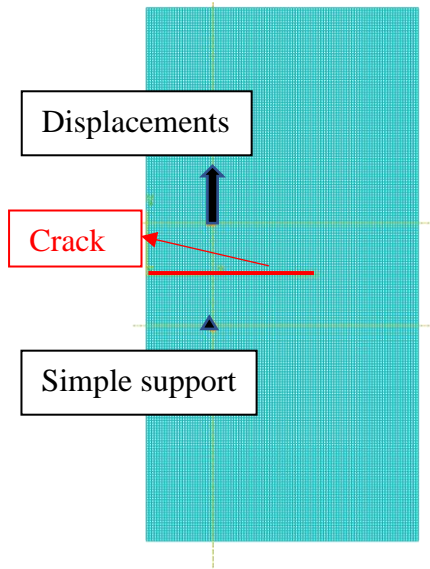
Fig. 11. VCCT analysis for OCT specimen.
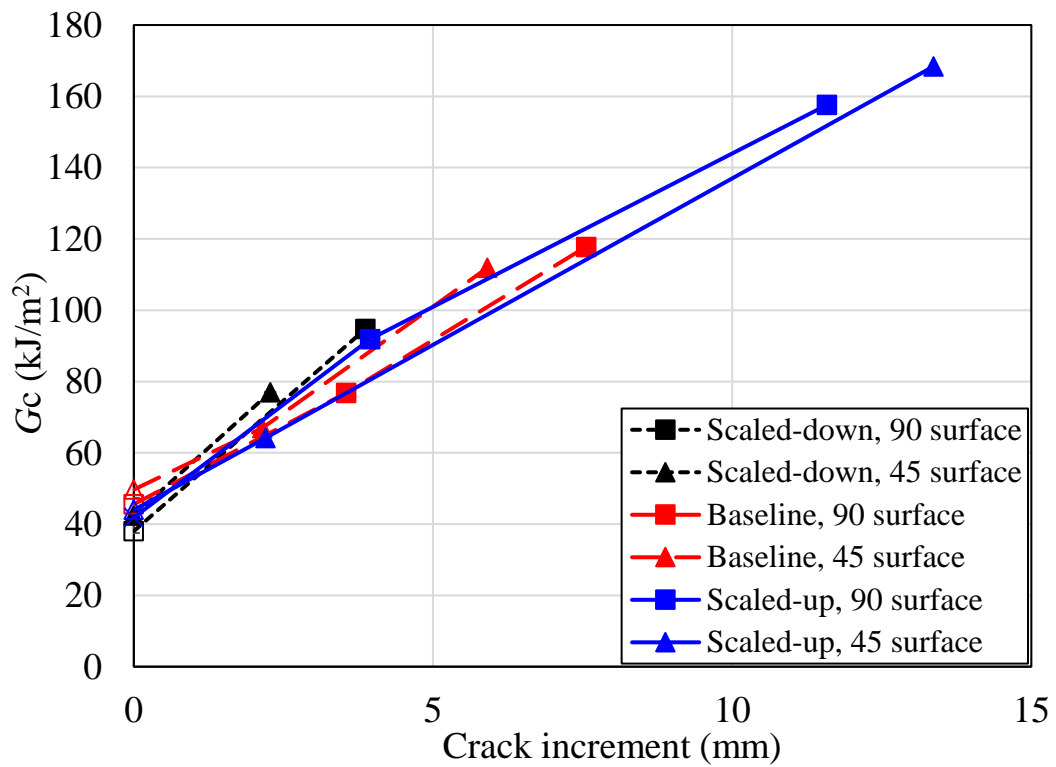
Fig. 12. Comparison of measured R-curves (open symbols represent repeated tests and solid symbols represent single interrupted tests).

Table 1. Average crack increments measured in the CT images of 0° plies (mm).

Layup / Size	[45/90/-45/0]$_{4s}$		[90/45/0/-45]$_{4s}$		
	1st large load drop	Major load drop	1st large load drop	Major load drop	Further load drop
Scaled-down	2.3	5.5	3.9	5.4	-
Baseline	2.2	5.9	3.6	7.6	-
Scaled-up	2.2	13.4	4.0	11.6	34.5